Lectures on Modelling and Simulation; A selection from AMSE # 2017-N°2; pp 62-75
Selection at the AMSE Conference Calcutta/India, November 4-5, 2017

Classification of Crossover Faults and Determining their Location in a Double Circuit Power Transmission System with Multiple Sources

*Nabamita Roy

*Assistant Professor, Electrical Engineering Department, MCKV Institute of Engineering, Liluah, Howrah, West Bengal, India (email: roynab@gmail.com)

Abstract

This paper presents a technique for identification and classification of short-circuit faults in case of double circuit transmission lines with different sources. The current signals at different terminals have been studied extensively. The signals of two terminals of the network have been chosen for feature extraction. Discrete S-Transform (DST) has been used for feature extraction from the current signals. These features have been used as input parameters for training a Probabilistic Neural Network (PNN) to identify the type of fault. Back Propagation Neural Network (BPNN) has been used for obtaining fault location. Double Line short-circuit and Double Line-Ground crossover faults have been simulated under different conditions. Satisfactory results have been obtained involving minimum time of computation and high accuracy. All the programming and simulations have been done in MATLAB environment

Key words

Back Propagation Neural Network (BPNN), Discrete S-Transform (DST), Fault, Fault identification and Classification, Feature selection, Probabilistic Neural Network (PNN),

1. Introduction

A fault is an inevitable phenomenon in a power system network. Uninterrupted power transmission is of utmost importance which requires a robust and accurate protection system.

Accurate, fast, and reliable fault classification technique is an important operational requirement in modern-day power transmission systems. On the other hand, the information of the type of fault is needed for fault location estimation. The soft computing techniques have shown relatively better performance in the method of fault classification with respect to speed and accuracy. The methods mainly involve the simulations of network and faults in reliable softwares like EMTP, PSCAD and MATLAB, involving the application of signal processing tools i,e, Wavelet transform and S-Transform.

The electrical power is transmitted either by single circuit system or double circuit system. Short circuit faults are quite common and in a double circuit system there remains a scope of crossover short-circuit in which two phases of different circuits are involved. Identification of such faults and determining their location is a challenging task.

A scheme of determination of fault location for a double circuit compensated transmission lines has been proposed in [1] where the location has been estimated by using Discrete Wavelet Transform (DWT) and KNN with less than 1 % error. A new approach of fault classification has been presented in [2] for EHV transmission lines using Rough Membership Neural network (RMNN). DWT has been used for feature extraction and a comparative analysis has been shown between RMNN and BPNN to establish that RMNN is faster and more accurate than BPNN as a classifier. The fault location has not been determined here. A hybrid method of ANN and DWT has been suggested in [3] for identification of faulty section and obtaining its location in a distribution network. The proposed method in this paper has been tested on a IEEE system but the effect of noise on the features extracted has not been discussed here. The paper [4] proposes an approach by combining independent component analysis (ICA) with travelling wave (TW) theory and Support Vector Machine (SVM) for fault analysis of HV Transmission lines. This method gives better performance in presence of noise. A new technique for fault location on transmission lines using only voltage measurements obtained from Wide Area Measurement Systems (WAMS) and the network bus admittance matrix has been reported in [5]. Fault classification has also been included in this paper using the same technique. In [6] inter-circuit shunt faults and cross-country faults in a double circuit system have been identified and classified using DWT and SVM. In this paper, the method of determining fault location and the effect of noise has not been discussed. A hybrid framework consisting of a proposed two-stage finite impulse response (FIR) filter, four support vector machines (SVMs), and eleven support vector regressions (SVRs) is implemented in [7] for classifying and locating short circuit faults in power

transmission lines. SVM has been also applied in [8] for fault classification in a long transmission line in which the features have been selected using wavelet packet transform.

In this paper, a method is proposed for identification of the type of fault and obtaining its corresponding location in a double circuit system. ANN has been involved here in which PNN is used for fault classification and BPNN for obtaining the fault location. The input features of both the PNN and BPNN have been obtained from DST of the current signals measured at any one terminal of the network. All the faults have been simulated in MATLAB environment. The scope of this paper is limited to the simulation of only double line short –circuit faults.

The rest of the paper is organized as follows. The simulation of faults in a double circuit network is described in section 2. DST is briefly discussed in section 3. The results of fault simulations and the extraction of features needed for fault analysis have been described in Section 4. Section 5 explains the method of fault classification and obtaining its location. The effect of noise has also been studied in this section.

2. Simulation of Faults and the System under study

A 3-phase double circuit power system network with three different sources has been simulated using the Simpower Toolbox of MATLAB-7 and is shown in Fig. 1. The length of each transmission line is 300 km.

System parameters:

Generator 1: Voltage = 220 kV, Three phase short-circuit level = 2250 MVA, X/R ratio = 15.

Generator 2: Voltage = 440 kV, Three phase short-circuit level = 4250 MVA, X/R ratio = 20.

Generator 3: Voltage = 132 kV, Three phase short-circuit level = 1250 MVA, X/R ratio = 10.

Transmission Lines 1&2: Length = 300 km, R_1 = 0.02336Ω/km, R_2 = 0.02336Ω/km, R_0 = 0.38848Ω/km, L_1 = 0.95106mH/km, L_2 = 0.95106mH/km, L_0 = 3.25083mH/km,

C_1 = 12.37nF/km, C_2 = 12.37nF/km, C_0 = 8.45 nF/km.

The sampling times of all the signals is taken to be 78.28 μs and the time period of simulation in MATLAB has been taken up to 0.04 secs. The sampling frequency is 12.8 kHz.

Crossover two phase short-circuit faults have been simulated in the following way as given below:

Double Line (L-L) Faults:

A_1A_2: Phase A of Line 1, A_1 shorted to phase A of line 2, A_2

A_1B_2: Phase A_1 of Line 1, A_1 shorted to phase B of line 2, B_2

A_1C_2: Phase A_1 of Line 1, A_1 shorted to phase C of line 2, C_2

B_1A_2: Phase B_1 of Line 1, B_1 shorted to phase A of line 2, B_2

B_1B_2: Phase B_1 of Line 1, B_1 shorted to phase B of line 2, B_2

B_1C_2: Phase B_1 of Line 1, B_1 shorted to phase C of line 2, C_2

C_1A_2: Phase C of Line 1, C_1 shorted to phase A of line 2, A_2

C_1B_2: Phase C of Line 1, C_1 shorted to phase B of line 2, B_2

C_1C_2: Phase C of Line 1, C_1 shorted to phase C of line 2, C_2

Double-Line-Ground faults have been simulated in the similar way.

Hence, the total number of the type of fault simulations (including both LL and LLG) is 18.

All the faults have been initiated at 19 different locations starting from B1, each being 10 km apart. The fault resistances considered for the simulation are from the range of 0-100Ω in steps of 20Ω. Fault inception angle is considered to be 0^0. The total number of fault simulations made in this system is 18×19×6 =2052.

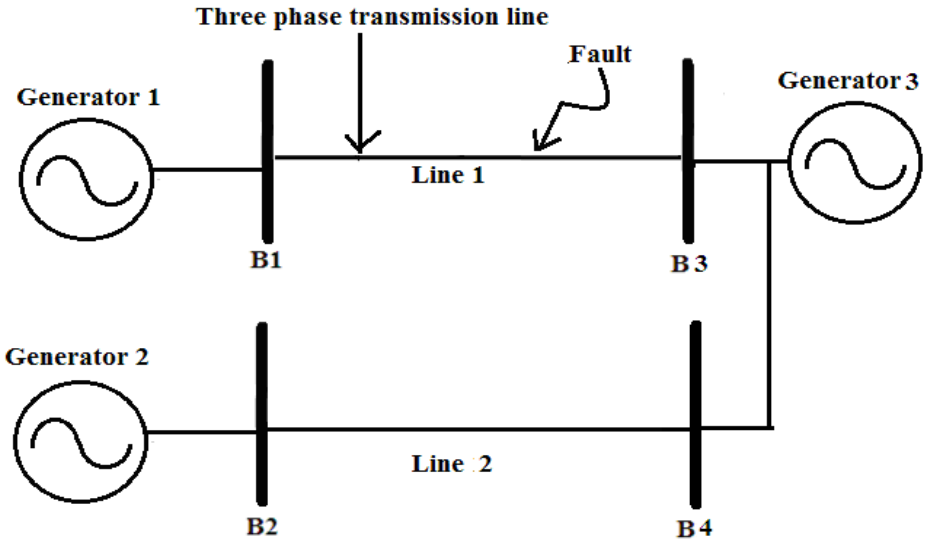

Fig.1: Single Line diagram of three phase double circuit network with three different sources

3. Discrete S-Transform (DST)

The S-Transform is an effectively efficient tool for time frequency representation (TFR) of a time series. ST is a hybrid of the STFT and WT and it produces a frequency dependent resolution with simultaneously localizing the real and imaginary spectra. Due to its easy interpretation, multi-resolution analysis and the ability of maintaining the meaningful local phase information, the ST has established successes in many areas including power quality, geophysics and biomedicine [9]. An electrical signal h(t) can be expressed in discrete form as h(kT), k = 0, 1, ……., N-1 and T is

the sampling time interval,[9,10].

The discrete Fourier transform of h(kT) is obtained as,

$$H\left[\frac{n}{NT}\right]=\frac{1}{N}\sum_{k=1}^{N-1}h(kT)e^{\frac{-i2\pi k}{N}} \tag{1}$$

Where n = 0,1,……..,N-1.

Using (4), the ST of a discrete time series is obtained by letting $f \to n/NT$ and $\tau \to jT$ as

$$S\left[jT,\frac{n}{NT}\right]=\sum_{m=0}^{N-1}H\left[\frac{m+n}{NT}\right]G(m,n)e^{i2\pi mj/N} \tag{2}$$

and $G(m,n)=e^{-2\pi^2m^2/n^2}$, $n\neq 0$ where j, m = 0,1,2,…….N-1 and n = 1,2,……N-1

Equation (2) generates a complex matrix (S-matrix) the rows of which are the frequencies, whereas the columns are the corresponding times. The amplitude of the ST spectrum is obtained from the absolute values of the complex matrix. Each column, thus, represents the local spectrum at one point in time. The matrix preserves the amplitude information of the frequency content of the signal at different resolutions.

4 Results of Simulation and Feature extraction from the current signals

The waveforms of the current signals for both A_1B_2G and A_1B_2 types of faults have been obtained from simulation at the busbars B1, B2, B3 and B4 and have been shown in Figs. [2]-[5] .

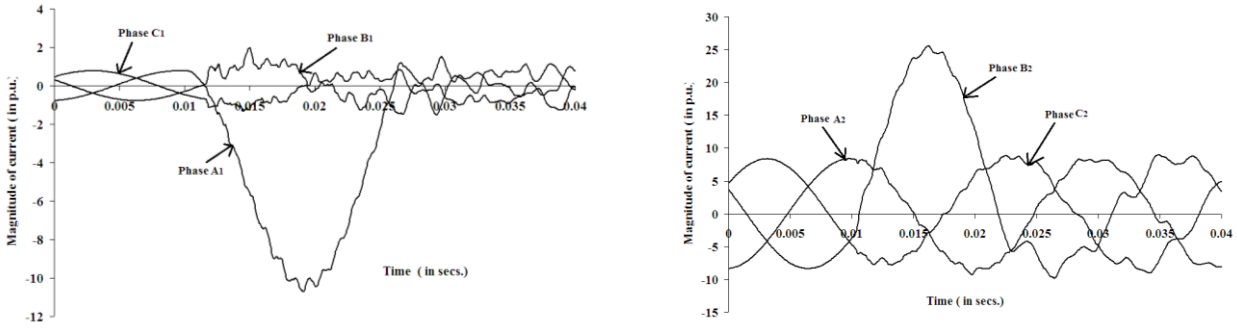

2 (a) 2(b)

Fig. 2 (a): Current waveforms of the three phases A_1, B_1, C_1 for a A_1B_2G type of fault at 100km from B_1 with $R_F = 0\ \Omega$ and fault inception angle = 0^0

2 (b): Current waveforms of the three phases A_2, B_2, C_2 for a A_1B_2G type of fault at 100km from B_2 with $R_F = 0\ \Omega$ and fault inception angle = 0^0.

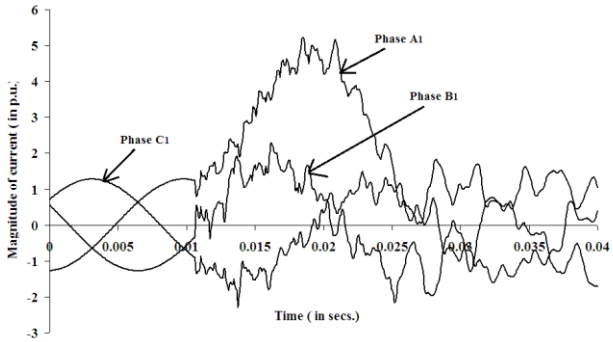

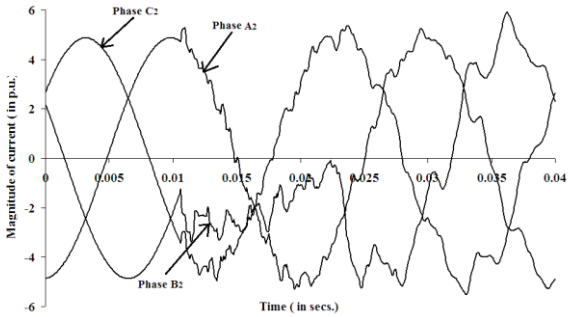

3(a) 3 (b)

Fig. 3 (a): Current waveforms of the three phases A_1, B_1, C_1 for a A_1B_2G type of fault at 100km from B_3 with $R_F = 0\ \Omega$ and fault inception angle = 0^0

Fig. 3 (b): Current waveforms of the three phases A_2, B_2, C_2 for a A_1B_2G type of fault at 100km from B_4 with $R_F = 0\ \Omega$ and fault inception angle = 0^0

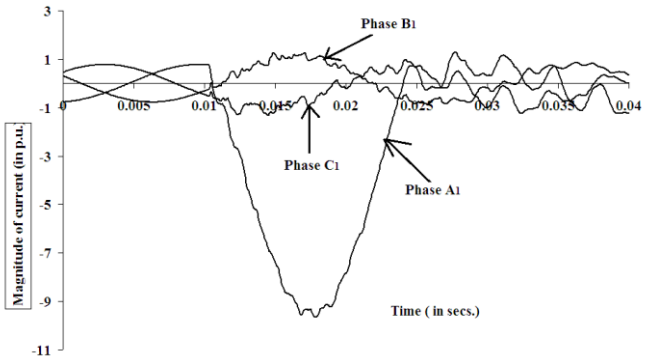

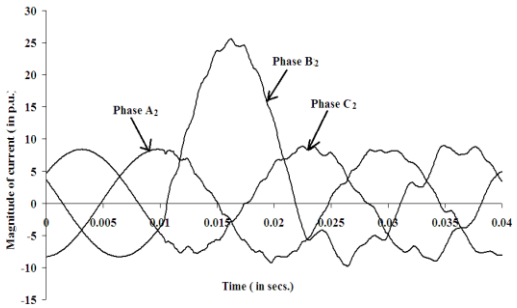

4(a) 4(b)

Fig. 4 (a): Current waveforms of the three phases A_1, B_1, C_1 for a A_1B_2 type of fault at 100km from B_1 with $R_F = 0\ \Omega$ and fault inception angle = 0^0

Fig. 4 (b): Current waveforms of the three phases A_2, B_2, C_2 for a A_1B_2 type of fault at 100km from B_2 with $R_F = 0\ \Omega$ and fault inception angle = 0^0

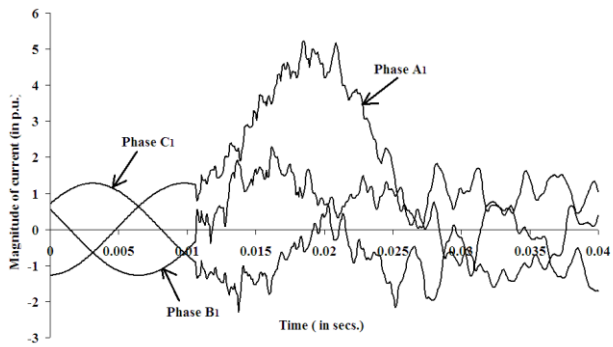

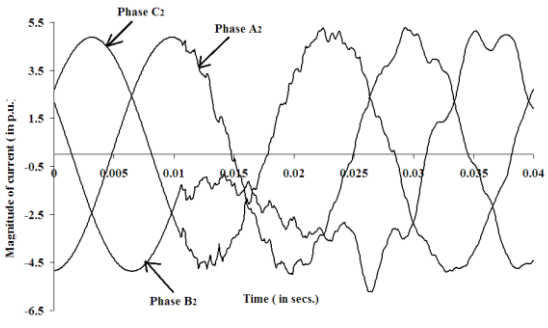

5(a) 5(b)

Fig. 5 (a): Current waveforms of the three phases A_1, B_1, C_1 for a A_1B_2 type of fault at 100km from B_3 with $R_F = 0\ \Omega$ and fault inception angle = 0^0

Fig. 5 (b): Current waveforms of the three phases A_2, B_2, C_2 for a A_1B_2 type of fault at 100km from B_4 with $R_F = 0\ \Omega$ and fault inception angle = 0^0

The current signals shown in Figs. [2-5] indicate that a fault has occurred in the network. But it is difficult to identify the type of fault from the signals. Henceforth, appropriate selection of feature is necessary.

4.1 Feature extraction

In this paper, two types of features (Xarea, Xpeak) have been obtained from the absolute values of S-matrices of all the current signals shown in figs. [2-5]

The feature Xarea for all the four terminals B1, B2, B3 and B4 have been obtained in the similar way as explained in [13] .

The other feature Xpeak has been obtained in the following steps as explained below:

- The sum of each column of the absolute value of the S-matrix is obtained along its entire row, producing a row matrix.
- The maximum value of this row matrix is considered as Xpeak.

The variation of the features Xarea and Xpeak for all the four terminals at different fault locations in case of A_1B_2G type of fault has been shown in Figs [6-7].

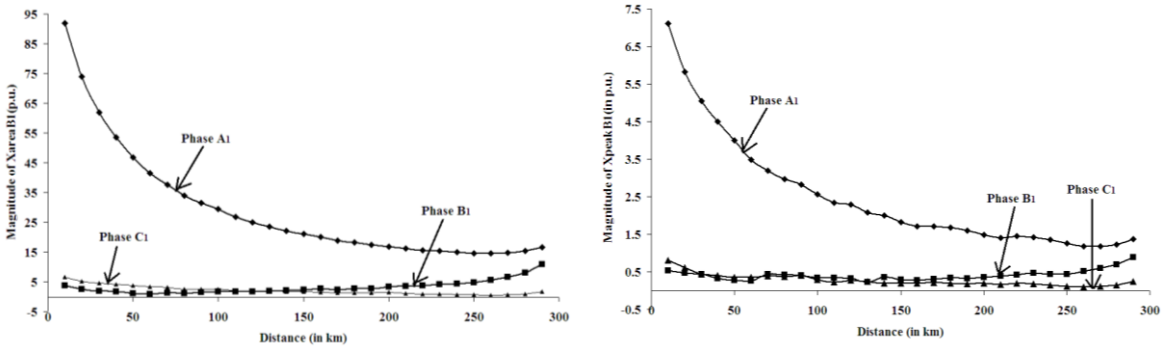

(a) (b)

Fig 6: Variation of magnitudes of the features (a) XareaB1 and (b) XpeakB1 for different fault locations in case of A_1B_2G type of fault

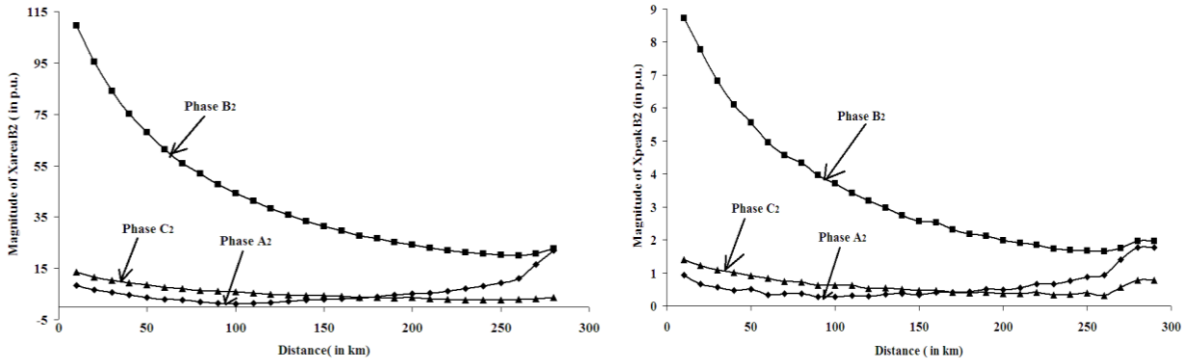

(a) (b)

Fig 7: Variation of magnitudes of the features (a) XareaB2 and (b) XpeakB2 for different fault locations in case of A_1B_2G type of fault

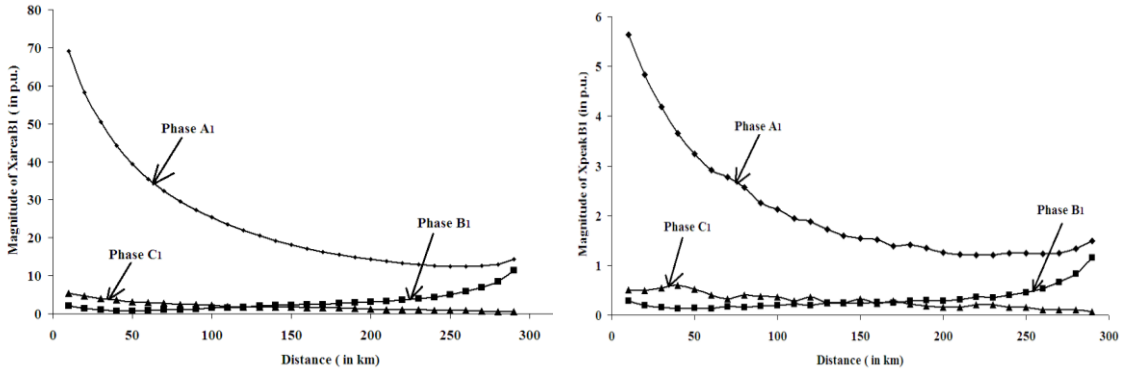

(a) (b)

Fig 8: Variation of magnitudes of the features (a) XareaB1 and (b) XpeakB1 for different fault locations in case of A_1B_2 type of fault

5. Fault Classification and Determination of fault location

5.1 Fault Classification

From the Figs [6]-[8] it is difficult to distinguish between A_1B_2G and A_1B_2 types of faults. Henceforth a suitable classification tool is necessary to identify the type of fault from the features. PNN is a fast and widely accepted ANN tool for classification purposes [13]. In this paper, the two types of features Xarea and Xpeak have been effectively trained by the PNN architecture for fault classification.

The features XareaB1, XpeakB1, XareaB2, XpeakB2 of the six phases have been used as input parameters. The magnitudes of the features for a few fault locations have been shown in Tables 1 and 2. The features of 10 current signals of each phase are used for training and the rest are used for testing purpose. The output of the PNN is summarised in Table 4. The average of correct predictions in case of LL faults and LLG faults is 98.5% and 98.6% respectively.

Table 1: Magnitudes of the features XareaB1 and XareaB2 in case of A_1B_2G type of fault

	Magnitude of XareaB1 (p.u.)			Magnitude of XareaB2 (p.u.)		
Fault Location (in km)	Phase A_1	Phase B_1	Phase C_1	Phase A_2	Phase B_2	Phase C_2
10	92.02	3.73	6.62	8.26	109.5	13.64
20	73.98	2.61	5.3	6.59	95.35	11.46
30	61.98	1.95	4.49	5.52	84.12	10.32
40	53.48	1.81	4.1	4.73	75.06	9.43
50	46.74	1.19	3.78	3.71	68.11	8.49
60	41.48	0.86	3.31	2.83	61.21	7.59
70	37.63	1.34	3.09	2.7	55.9	7.19
80	33.99	1.21	2.6	1.97	51.85	6.47
90	31.57	1.56	2.62	1.53	47.61	6.11
100	29.51	1.77	2.56	1.21	44.28	5.92
110	26.81	1.64	1.99	1.34	41.28	5.27
120	25.04	1.83	1.98	1.68	38.42	4.98
130	23.48	1.92	1.84	2.24	35.88	4.59
140	22.15	2.23	1.73	2.55	33.39	4.41
150	21.16	2.36	1.66	2.89	31.25	4.35
160	20.01	2.66	1.61	3.24	29.65	4.17
170	18.84	2.43	1.33	3.44	27.75	3.6
180	18.19	2.73	1.42	4.02	26.55	3.55
190	17.45	2.79	1.4	4.64	25.29	3.3
200	16.84	3.37	1.63	5.03	24.27	3.59

Table 2: Magnitudes of the features XpeakB1 and XpeakB2 in case of A_1B_2G type of fault

	Magnitude of XpeakB1 (p.u.)			Magnitude of XpeakB2 (p.u.)		
Fault Location (in km)	Phase A_1	Phase B_1	Phase C_1	Phase A_2	Phase B_2	Phase C_2
10	7.12	0.53	0.8	0.93	8.72	1.39
20	5.82	0.47	0.61	0.66	7.77	1.22
30	5.05	0.44	0.44	0.56	6.82	1.08
40	4.5	0.32	0.41	0.47	6.11	1.01
50	4	0.28	0.36	0.5	5.55	0.92
60	3.49	0.26	0.36	0.34	4.95	0.84
70	3.19	0.44	0.38	0.37	4.57	0.74
80	2.96	0.42	0.37	0.37	4.33	0.71
90	2.83	0.41	0.4	0.28	3.97	0.63
100	2.57	0.34	0.29	0.28	3.71	0.63
110	2.34	0.34	0.22	0.31	3.43	0.62
120	2.29	0.33	0.28	0.29	3.18	0.53
130	2.08	0.22	0.25	0.35	2.98	0.55

140	2	0.36	0.19	0.36	2.75	0.5
150	1.82	0.29	0.2	0.34	2.56	0.46
160	1.71	0.27	0.2	0.41	2.53	0.47
170	1.71	0.31	0.21	0.4	2.31	0.41
180	1.67	0.34	0.2	0.43	2.18	0.38
190	1.59	0.32	0.18	0.5	2.12	0.4
200	1.49	0.35	0.19	0.49	1.99	0.37

Table 3: Magnitudes of the features XpeakB1 and XpeakB1 in case of A_1B_2 type of fault

	Magnitude of XareaB1 (p.u.)			Magnitude of XpeakB1 (p.u.)		
Fault Location (in km)	Phase A_1	Phase B_1	Phase C_1	Phase A_1	Phase B_1	Phase C_1
10	69.11	2.12	5.44	5.64	0.28	0.51
20	58.31	1.45	4.62	4.84	0.2	0.49
30	50.38	0.96	4	4.18	0.16	0.55
40	44.23	0.61	3.58	3.66	0.13	0.59
50	39.39	0.62	3.17	3.24	0.14	0.52
60	35.48	0.83	3.01	2.92	0.13	0.4
70	32.24	1	2.7	2.77	0.17	0.33
80	29.57	1.05	2.43	2.57	0.16	0.4
90	27.3	1.23	2.4	2.26	0.18	0.37
100	25.4	1.54	2.33	2.12	0.19	0.36
110	23.48	1.59	1.98	1.95	0.22	0.28
120	21.9	1.73	1.7	1.88	0.2	0.36
130	20.63	2	1.71	1.72	0.24	0.24
140	19.24	2.17	1.73	1.59	0.24	0.25
150	18.12	2.2	1.68	1.54	0.23	0.32
160	17.14	2.4	1.51	1.51	0.26	0.23
170	16.27	2.5	1.64	1.39	0.25	0.29
180	15.58	2.69	1.57	1.41	0.29	0.22
190	14.92	2.91	1.38	1.35	0.3	0.18
200	14.26	3.04	1.25	1.26	0.29	0.16

Table 4: Results of fault classification from the PNN

Type of Fault	PNN output	% of correct predictions	Type of Fault	PNN output	% of correct predictions
A_1A_2	1	97.6	A_1A_2G	10	97.8
A_1B_2	2	97.9	A_1B_2G	11	97.9
A_1C_2	3	98.5	A_1C_2G	12	98.7

B_1A_2	4	98.0	B_1A_2G	13	97.8
B_1B_2	5	99.4	B_1B_2G	14	99.5
B_1C_2	6	98.4	B_1C_2G	15	98.5
C_1C_2	7	99.5	C_1C_2G	16	98.9
C_1B_2	8	97.6	C_1B_2G	17	98.7
C_1A_2	9	99.6	C_1A_2G	18	99.5
			No fault	19	99.6

5.2 Determination of fault location

The fault location has been obtained from a BPNN. Properly trained backpropagation networks tend to give reasonable answers when presented with inputs that they have never seen [13]**.** Once the short-circuited phases have been identified from the PNN, the parameter Xarea or Xpeak of any one of the faulty phases has been used as the input feature as the pattern of variation of both the parameters with respect to fault location is almost same. In case of A_1B_2G and A_1B_2 type of faults, the features XareaB1 obtained corresponding to phase A_1 for different fault locations have been used for training the BPNN. The features of 10 current signals have been used for training and the rest are used for testing purpose. Levenberg–Marquardt (LM) algorithm has been used for training the BPNN. The percentage error is calculated during estimation of fault location as shown in Table 5 and according to equation (3). Table 5 show the results of fault location obtained from the BPNN in case of A_1B_2 type of fault.

$$\frac{ActualFaultLocation - BPNNoutput}{ActualFaultLocation} \times 100 \qquad (3)$$

The maximum error achieved in obtaining fault location is 1.03% and 1.43% for LL and LLG faults respectively.

Table 5: Fault location in case of A_1B_2 and A_1B_2G type of fault with Fault resistance, $R_F = 0\Omega$

Type of fault: A_1B_2			Type of fault: A_1B_2G		
Actual Fault Location (km)	BPNN output (km)	% error	Actual Fault Location (km)	BPNN output (km)	% error
15	14.95	0.33	15	15.05	-0.33
25	25.12	-0.48	25	25.12	-0.48

35	34.64	1.03	35	35.50	-1.43
45	45.05	-0.11	45	45.21	-0.47
55	55.05	-0.09	55	55.12	-0.22
65	64.56	0.68	65	65.56	-0.86
75	75.32	-0.43	75	75.12	-0.16
85	85.43	-0.51	85	85.03	-0.04
95	95.15	-0.16	95	95.25	-0.26
105	105.40	-0.38	105	105.40	-0.38

.

5.3 Implementation of noisy signals

The current signals obtained at the Bus B1 and Bus B2 from simulation for both LL and LLG faults have been impregnated with 20dB white Gaussian noise by programming in MATLAB. The variation of the features XareaB1 and XpeakB1 with respect to fault location have been plotted in Fig. 9 in presence of noise. From Fig. 9 it is observed that the profile of variation of both the features is same with that of the Figs. [6-8]. The results of classification and estimation of fault location have been given in Tables 6 and 7. The average of correct classifications from PNN is 98.4% and 98.5 % in case of LL and LLG faults respectively. The maximum error achieved in obtaining fault location is 2.05% and 2.43% for LL and LLG faults respectively.

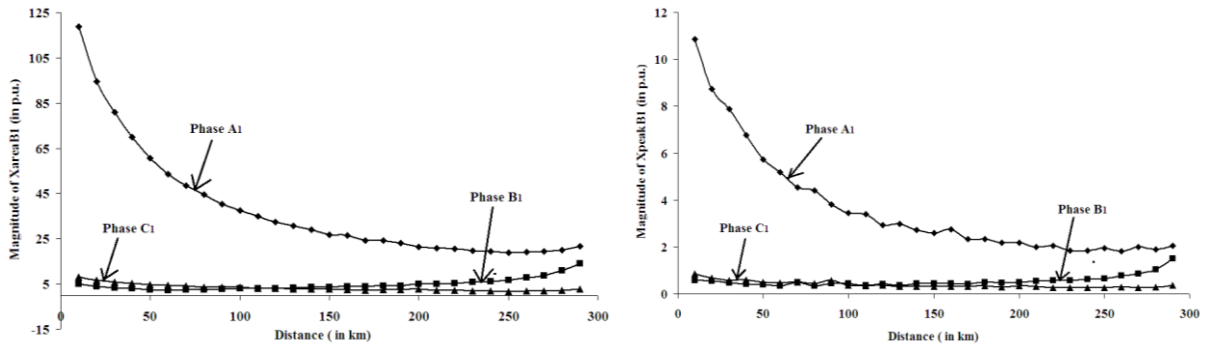

(a) (b)

Fig 9: Variation of magnitudes of the features (a) XareaB1 and (b) XpeakB1 for different fault locations in case of A_1B_2G type of fault with noisy current signals

Conclusion

The accuracy of fault classification depends largely on the appropriate selection of features from the current/voltage signals of a power system network. In this paper, only the current signals of two terminals of the network have been used for extracting features. Twelve features (two for

each line) are needed for the six lines to identify the affected phases from PNN. Only one feature of the affected phase is needed for obtaining fault location from the BPNN. The faults have been simulated at different locations with variation in fault resistance. The effect of noise has also been studied. The average percentage of correct classifications from the PNN is in the range of 98.4-98.6% including the presence of noise in the current signals. The faults have been located by the BPNN with the maximum error lying in the range of 1.03%-2.43% considering the presence /absence of noise. The results indicate that the proposed method of fault classification and estimation of fault location can be effectively implemented for other multi-terminal systems as well.

The present work can be further extended for the analysis of Line-Ground faults, and Three phase short-circuit faults in which phases of different circuits are also involved.

References

1. Aleena Swetapadma, Praveen Mishra, Anamika Yadav, Almoataz Y. Abdelaziz, "A non-unit protection scheme for double circuit series capacitor compensated transmission lines", Electric Power Systems Research, Vol. 148, July 2017, Pages 311–325, https://doi.org/10.1016/j.epsr.2017.04.002.
2. Zhengyou He, Sheng Lin', Yujia Deng, Xiaopeng Li, Qingquan Qian, "A rough membership neural network approach for fault classification in transmission lines" , International Journal of Electrical Power & Energy Systems, Volume 61, October 2014, Pages 429–439, https://doi.org/10.1016/j.ijepes.2014.03.027.
3. Adeyemi Charles Adewole, Raynitchka Tzoneva, Shaheen Behardien, "Distribution network fault section identification and fault location using wavelet entropy and neural networks", Applied Soft Computing, Vol. 46, September 2016, Pages 296–306, https://doi.org/10.1016/j.asoc.2016.05.013.
4. A.R. Almeida , O.M. Almeida, B.F.S. Junior, L.H.S.C. Barreto, A.K. Barros, "ICA feature extraction for the location and classification of faults in high-voltage transmission lines", Electric Power Systems Research, Volume 148, July 2017, Pages 254–263, https://doi.org/10.1016/j.epsr.2017.03.030.
5. Sayari Das, Shiv P. Singh, Bijaya K. Panigrahi, "Transmission line fault detection and location using Wide Area Measurements", Electric Power Systems Research, Vol. 151, October 2017, Pages 96–105, https://doi.org/10.1016/j.epsr.2017.05.025.

6. Aleena Swetapadma , Anamika Yadav, “Directional relaying using support vector machine for double circuit transmission lines including cross-country and inter-circuit faults”, International Journal of Electrical Power & Energy Systems, Volume 81, October 2016, Pages 254–264, https://doi.org/10.1016/j.ijepes.2016.02.034.
7. Hassan Fathabadi, “Novel filter based ANN approach for short-circuit faults detection, classification and location in power transmission lines”, International Journal of Electrical Power & Energy Systems, Volume 74, January 2016, Pages 374–383, https://doi.org/10.1016/j.ijepes.2015.08.005.
8. Papia Ray, Debani Prasad Mishra, “Support vector machine based fault classification and location of a long transmission line”, Engineering Science and Technology, an International Journal, Vol. 19, Issue 3, September 2016, Pages 1368–1380, https://doi.org/10.1016/j.jestch.2016.04.001.
9. F. Zhao and R. Yang, “Localization of the Complex Spectrum: S-Transform”, IEEE Trans. On Signal Processing, vol. 44, No. 4, pp. 998-1001, April 1996
10. Stockwell, RG (1999), “S -Transform Analysis of Gravity Wave Activity from a Small Scale Network of Airglow Imagers”, PhD thesis, University of Western Ontario, London, Ontario, Canada.
11. S. Mishra, C. N. Bhende, and B. K. Panigrahi, “Detection and Classification of Power Quality Disturbances Using S-Transform and Probabilistic Neural Network”, IEEE Trans. On Power Delivery, Vol. 23, No. 1, pp. 280-287, Jan 2008.
12. Howard Demuth, Mark Beale, Neural Network Toolbox User’s Guide , Version 4, copyright 1992 - 2001 by The MathWorks, Inc.
13. Nabamita Roy, “Identification of Cross-over Short-circuit Faults and Determining their location in a Double Circuit Power Transmission System”, Association for the Advancement of Modelling and Simulation Techniques in Enterprises , Proc. of MS-17, India, Nov 4-5, 2017.